



Article

# Nanostructured Polymethylsiloxane/Fumed Silica Blends

Iryna Protsak <sup>1,2</sup>, Volodymyr M. Gun'ko <sup>3</sup>, Volodymyr V. Turov <sup>3</sup>, Tetyana V. Krupska <sup>3</sup>, Eugeniy M. Pakhlov <sup>3</sup>, Dong Zhang <sup>4</sup>, Wen Dong <sup>1,\*</sup> and Zichun Le <sup>2</sup>

<sup>1</sup> College of Environment, Zhejiang University of Technology, Hangzhou 310014, China

<sup>2</sup> College of Science, Zhejiang University of Technology, Hangzhou 310023, China

<sup>3</sup> Chuiko Institute of Surface Chemistry of National Academy of Sciences of Ukraine, Kyiv 03164, Ukraine

<sup>4</sup> Department of Chemical & Biomolecular Engineering, University of Akron, Akron, OH 44325, USA

\* Correspondence: dongwen@zjut.edu.cn

Received: 27 June 2019; Accepted: 26 July 2019; Published: 28 July 2019



**Abstract:** Polymethylsiloxane (PMS) and fumed silica, alone and in a blended form (1:1 w/w), differently pretreated, hydrated, and treated again, were studied using TEM and SEM, nitrogen adsorption–desorption, <sup>1</sup>H MAS and <sup>29</sup>Si CP/MAS NMR spectroscopy, infrared spectroscopy, and methods of quantum chemistry. Analysis of the effects of adding water (0–0.5 g of water per gram of solids) to the blends while they are undergoing different mechanical treatment (stirring with weak (~1–2 kg/cm<sup>2</sup>) and strong (~20 kg/cm<sup>2</sup>) loading) show that both dry and wetted PMS (as a soft material) can be grafted onto a silica surface, even with weak mechanical loading, and enhanced mechanical loading leads to enhanced homogenization of the blends. The main evidence of this effect is strong nonadditive changes in the textural characteristics, which are 2–3 times smaller than additive those expected. All PMS/nanosilica blends, demonstrating a good distribution of nanosilica nanoparticles and their small aggregates in the polymer matrix (according to TEM and SEM images), are rather meso/microporous, with the main pore-size distribution peaks at  $R > 10$  nm in radius and average  $\langle R_V \rangle$  values of 18–25 nm. The contributions of nanopores ( $R < 1$  nm), mesopores ( $1 \text{ nm} < R < 25 \text{ nm}$ ), and macropores ( $25 \text{ nm} < R < 100 \text{ nm}$ ), which are of importance for studied medical sorbents and drug carriers, depend strongly on the types of the materials and treatments, as well the amounts of water added. The developed technique (based on small additions of water and controlled mechanical loading) allows one to significantly change the morphological and textural characteristics of fumed silica (hydrocompaction), PMS (drying–wetting–drying), and PMS/A-300 blends (wetting–drying under mechanical loading), which is of importance from a practical point of view.

**Keywords:** polymethylsiloxane/nanosilica blends; hydration effect; mechanical loading effect; textural characteristics; interfacial layer structure

## 1. Introduction

Silicas can easily be modified to significantly change many important characteristics of the materials [1–16]. Various functionalized silicas (fumed nanosilica, silica gels, precipitated silicas, ordered mesoporous silicas, etc.) and siloxane-based polymers (e.g., linear polydimethylsiloxane, PDMS, 3D-cross-linked polymethylsiloxane (PMS)) are widely used in industry and medicine as well in various branches of science [1–23]. One of the main characteristics of these materials is their degree of hydrophobicity, which allows their interactions with various liquids, polymers, and solids to be controlled. PMS, as a 3D-cross-linked polymer with one CH<sub>3</sub> group attached to each Si atom and residual silanols [21–23], may be considered as an intermediate between PDMS and methylated nanosilica containing residual silanols [1,2,24–28]. In a series of nanostructured silicas with surface functionalities,

such as  $-\text{O})_3\text{SiCH}_3$ ,  $-\text{O})_2\text{Si}(\text{CH}_3)_2$ , and  $-\text{O}-\text{Si}(\text{CH}_3)_3$ , the degree of hydrophobicity increases, i.e., PMS is less hydrophobic than PDMS. There is a commercial hydrogel with PMS incompletely cross-linked and containing a certain amount of residual silanols (a medicinal sorbent entitled Enterosgel, it contains 7–8 wt.% of PMS and 93–92 wt.% of water, is produced by Kreoma-Pharm, Ukraine, and it is also used as a drug carrier), which represents a gel-like soft material [29,30]. However, pure PDMS is hydrophobic (there are no silanols, and the siloxane bonds tend to be low-polar bonds) and cannot form hydrogels. Note that the Si–O–Si bonds are relatively flexible due to small changes in the energy which follow upon changes in the  $\angle\text{SiOSi}$  angle in the 140 to 180° range [1,2]. Amorphous silicas are therefore relatively stable despite certain differences in 3–8-member siloxane rings (characterized various values of  $\angle\text{SiOSi}$ ) formed upon the synthesis. Clear, PMS is less flexible than PDMS, but PMS is soft because only three bonds from four ones of each Si atom can take part in cross-linking [29,30].

Clear, the properties and characteristic of any nanostructured composites strongly depend on the distributions (uniform – nonuniform, nanolayers – nanoclusters – nanodomains – microdomains – monolith fragments) of different components in the composites. These effects could be stronger (especially upon interaction with water [31–37]) for the composites with nanostructured hydrophilic and hydrophobic components [38,39]. Using specific treatments and certain (rather small) amounts of water, it is possible to prepare hydrophilic blends with hydrophobic and hydrophilic components. Subsequent treatments (e.g., drying) of these blends allow one to obtain hydrophobic composites, the hydrophilic properties of which can renew after additional treatment (e.g., wetting and stirring or grinding at greater mechanical loading) [38,39].

Fumed nanosilica and Enterosgel are used in medical applications not only as sorbents but also as drug carriers [17,29,30,40]. Therefore, changes in the textural characteristics of the drug carriers can strongly affect the drug release upon the medical applications of the drug delivery systems. The textural and hydrophilic/hydrophobic characteristics of the blends of nanosilica and PMS could be strongly changed and better controlled than those of individual sorbents due to their morphological, textural, and structural features.

Fumed nanosilica and PMS are soft-powder materials because their aggregates of nanoparticles and agglomerates of aggregates may be easily rearranged under any treatment [36]. The results of these treatments depend on several factors such as the (i) hydrational, thermal, and mechanical history of the components; (ii) the weight ratio of the components; (iii) the amounts of added water; (iv) the mechanical loading; (v) the time of treatment; and (vi) the temperature [1,2,24–26,36–41]. In this study, two important factors, namely, a small amount of added water and the type of mechanical loading upon stirring of the PMS/nanosilica blends, are analyzed to control the characteristics of the final blends.

## 2. Materials and Methods

### 2.1. Materials

Commercial polymethylsiloxane (PMS) hydrogel (Enterosgel, hPMS, Kreoma-Pharm, Ukraine, ~7–8 wt.% of PMS and 93–92 wt.% of water) and dry PMS (dPMS) were used as the initial materials. Note that after drying of Enterosgel at room temperature for a week, the amount of residual water bound in PMS is small (~0.7 wt.%), i.e., the material becomes rather hydrophobic. Fumed silica (nanosilica) A-300 (Pilot plant of Chuiko Institute of Surface Chemistry, Kalush, Ukraine) was mixed with water (1:5) and dried at 160 °C for several hours, resulting in hydrocompacted nanosilica (cA-300) [41], with increased bulk density ( $\rho_b$ ) toward 0.25 g/cm<sup>3</sup>, since the initial A-300 has  $\rho_b \approx 0.05$  g/cm<sup>3</sup>.

Dry PMS (dPMS) and dry cA-300 (1:1 w/w) powders were mixed in a porcelain mortar for 5 min without strong mechanical loading (sample 1, B1). Distilled water ( $h = 0.1$  g per gram of solids) was then added and the blend was stirred without (5 min, sample 2, Bh1) or with (10 min, sample 3, Bh1s) strong mechanical loading. Water ( $h = 0.2$  g/g) was added to S1, and the sample was stirred without strong mechanical loading (sample 4, Bh2). Bh2 was additionally stirred with strong mechanical loading for 10 min (sample 5, Bh2s). Sample 6 (Ad1) corresponds to dried and stirred cA-300 (Ad1).

Sample 7 (Pdl) corresponds to stirred dPMS. Sample 8 (Phdl) is hPMS-dried for a week (in sample labels: A is cA-300, B is the blend of dPMS and cA-300, l is low mechanical loading ( $\sim 1 \text{ kg/cm}^2$ ) upon simple mixing of samples, s is strong mechanical loading ( $\sim 20 \text{ kg/cm}^2$ ) upon mixing, d is dried samples, and h is hydrated samples at  $h = 0.1 \text{ g/g}$  (h1) or  $0.2 \text{ g/g}$  (h2)).

## 2.2. Transmission (TEM) and Scanning (SEM) Electron Microscopy

TEM (TECNAI G2 F30 microscope (FEI–Philips, Amsterdam, The Netherlands), operating voltage 300 kV) was used to analyze the particulate morphology of samples (Figure 1 and Figures S1 and S2 in Electronic Supplementary Material (ESM) file). The powder samples were added to acetone (chromatographic grade) and sonicated. A suspension drop was then deposited onto a copper grid covered by a thin carbon film. After acetone evaporation, the dry sample remaining on the film was studied.

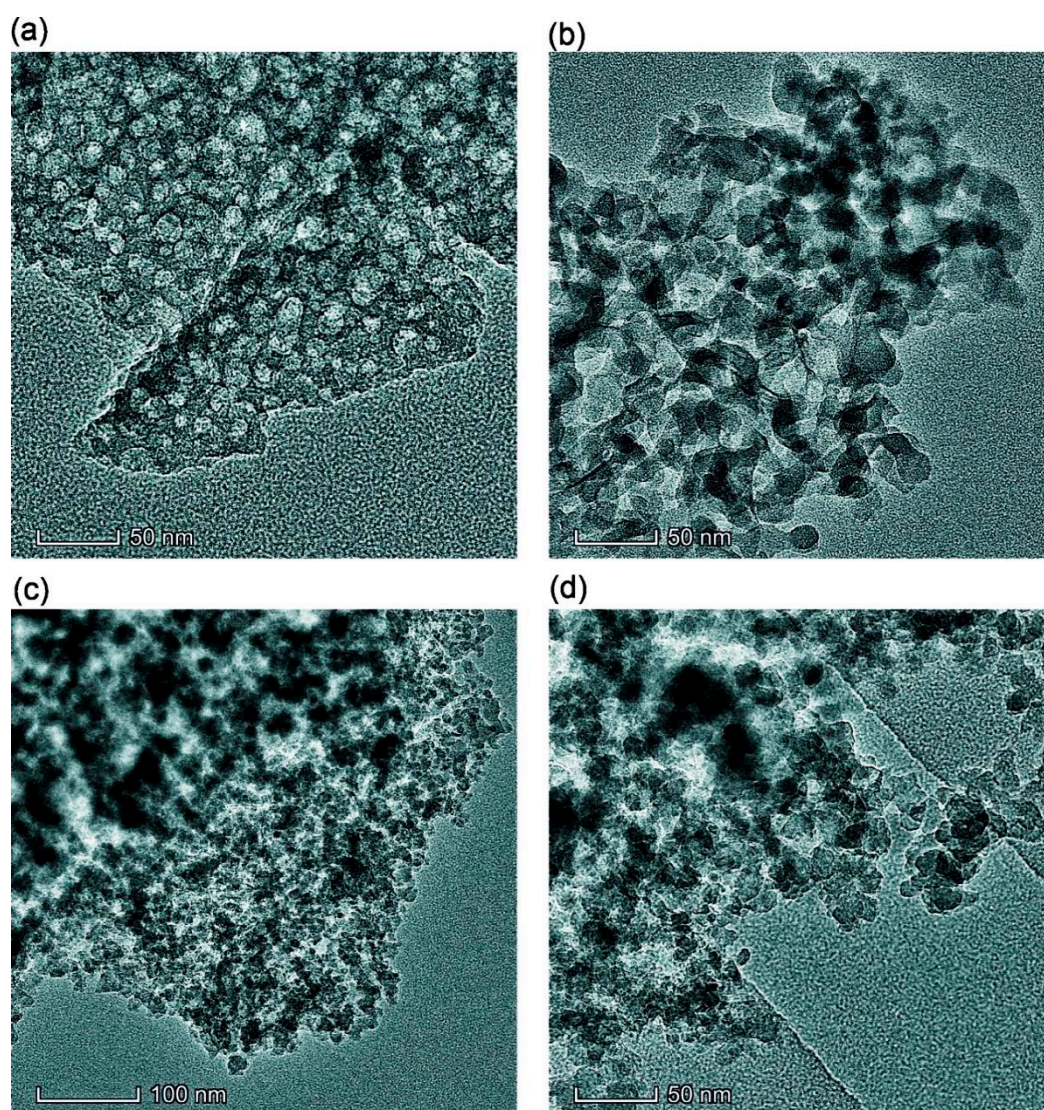


**Figure 1.** TEM images of samples (a) Bl, (b) Bh2s, (c) Adl, and (d) Pdl (scale bar 50 nm (a, b, d) and 100 nm (c)).

SEM (FE–SEM, Hitachi S–4700, Tokyo, Japan, operating voltage of 15 kV, and magnification of  $\times 5000$ – $100000$ ) (Figure 2, Figures S3 and S4) was used to analyze the morphological features of the dried powder samples.

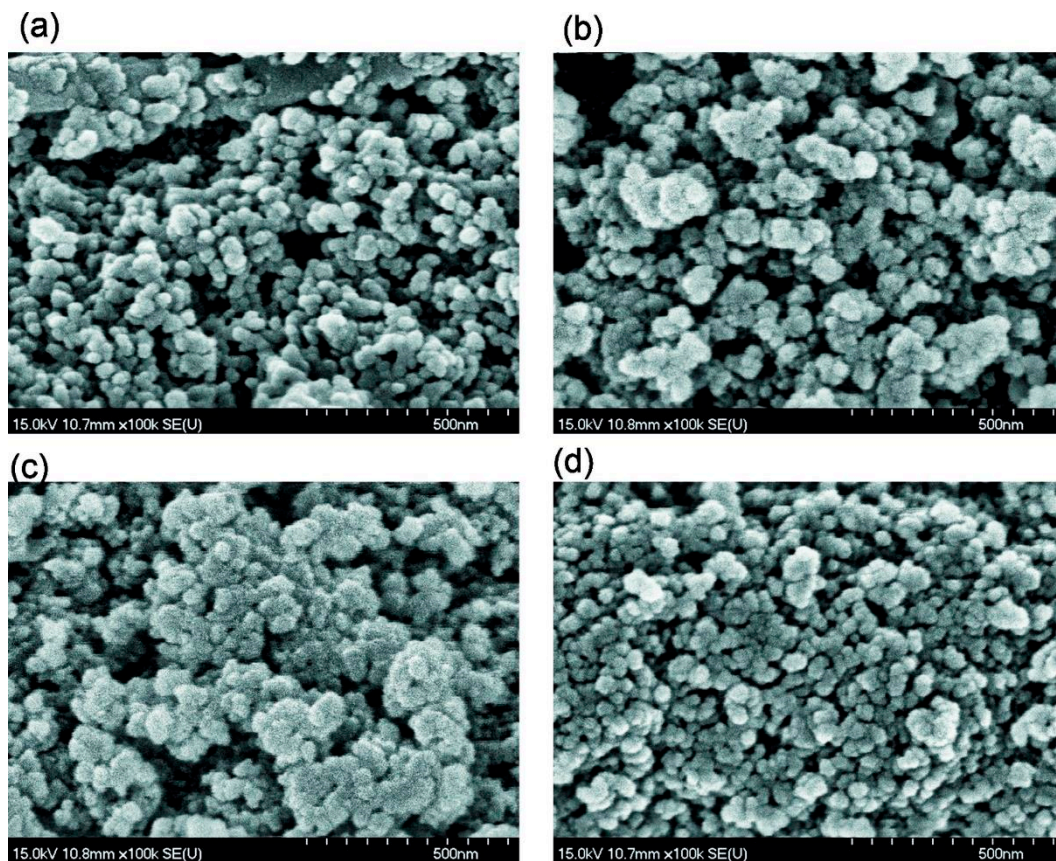


Figure 2. SEM images of (a) Bl, (b) Bh2s, (c) Adl, and (d) Pdl (scale bar 500 nm).

### 2.3. Textural Characteristics

To analyze the textural characteristics of individual and mixed samples degassed at 110 °C for 12 h (Table 1), low-temperature (77.4 K) nitrogen adsorption–desorption isotherms (Figure S5 in ESM file) were recorded using a Micromeritics ASAP 2460 adsorption analyzer (Micromeritics, Norcross, GA, USA). The specific surface area (Table 1,  $S_{\text{BET}}$ ) was calculated according to the standard BET method at  $0.05 < p/p_0 < 0.3$  (using Micromeritics software), where  $p$  and  $p_0$  denote the equilibrium and saturation pressure of nitrogen at 77.4 K, respectively [42]. The total pore volume (Table 1,  $V_p$ ) was estimated from the nitrogen adsorption at  $p/p_0 \approx 0.98\text{--}0.99$  [43]. The nitrogen desorption data were used to compute the pore-size distributions (PSD) (differential  $f_V(R) \sim dV_p/dR$  and  $f_S(R) \sim dS/dR$ ) using a self-consistent regularization (SCR) procedure under non-negativity condition ( $f_V(R) \geq 0$  at any pore radius  $R$ ) at a fixed regularization parameter  $\alpha = 0.01$  (Figure 3) [44]. A complex pore model including slit-shaped (S) and cylindrical (C) pores and voids (V) between spherical particles packed in random aggregates (SCV/SCR method) was applied [44]. The differential PSD with respect to the pore volume  $f_V(R) \sim dV/dR$ ,  $\int f_V(R)dR \sim V_p$  were recalculated to incremental PSD (IPSD) at  $\Phi_V(R_i) = (f_V(R_{i+1}) + f_V(R_i))(R_{i+1} - R_i)/2$  at  $\sum \Phi_V(R_i) = V_p$  for a better view of the PSD at large  $R$  values. The  $f_V(R)$  and  $f_S(R)$  functions were used to calculate contributions of nanopores ( $V_{\text{nano}}$  and  $S_{\text{nano}}$  at  $0.35 \text{ nm} < R < 1 \text{ nm}$ ), mesopores ( $V_{\text{meso}}$  and  $S_{\text{meso}}$  at  $1 \text{ nm} < R < 25 \text{ nm}$ ), and macropores ( $V_{\text{macro}}$  and  $S_{\text{macro}}$  at  $25 \text{ nm} < R < 100 \text{ nm}$ ) [44]. The average values of the pore radii (Table 1) were determined with respect to the pore volume ( $X = V$ ) and specific surface area ( $X = S$ ) as the corresponding moments of the distribution functions:

$$\langle R_X \rangle = \frac{\int_{R_{\min}}^{R_{\max}} R f_X(R) dR}{\int_{R_{\min}}^{R_{\max}} f_X(R) dR} \quad (1)$$

**Table 1.** Textural characteristics of PMS, A-300, and their blends (SCV/SCR method).

No	Sample Composition	Sample Label	$S_{BET}$ (m <sup>2</sup> /g)	$S_{DFT,cyl}$ (m <sup>2</sup> /g)	$S_{nano}$ (m <sup>2</sup> /g)	$S_{meso}$ (m <sup>2</sup> /g)	$S_{macro}$ (m <sup>2</sup> /g)	$V_p$ (cm <sup>3</sup> /g)	$V_{nano}$ (cm <sup>3</sup> /g)	$V_{meso}$ (cm <sup>3</sup> /g)	$V_{macro}$ (cm <sup>3</sup> /g)	$\langle R_V \rangle$ (nm)	$\langle R_S \rangle$ (nm)	$c_{slit}$	$c_{cyl}$	$c_{void}$
1	dPMS/cA-300	B1	186	164	52	124	10	0.788	0.026	0.594	0.168	19.65	7.57	0.699	0.221	0.080
2	dPMS/cA-300	Bh1l	166	152	38	107	22	0.827	0.012	0.463	0.352	24.17	9.69	0.162	0.798	0.041
3	dPMS/cA-300	Bh1s	165	151	34	108	23	0.848	0.011	0.461	0.376	25.13	10.27	0.171	0.774	0.055
4	dPMS/cA-300	Bh2l	159	150	31	113	14	0.691	0.011	0.433	0.247	23.51	8.44	0.200	0.740	0.060
5	dPMS/cA-300	Bh2s	134	127	32	97	5	0.613	0.018	0.506	0.089	18.37	7.60	0.775	0.136	0.089
6	cA-300	Adl	278	278	77	201	1	1.304	0.038	1.243	0.024	13.39	7.19	0.794	0.190	0.016
7	dPMS	Pdl	453	459	83	319	52	1.808	0.049	0.916	0.843	25.26	7.86	0.396	0.302	0.302
8	PMS initial	Phdl	98	99	19	71	8	0.390	0.011	0.234	0.145	25.41	7.62	0.437	0.249	0.315
9	A-300 initial	A-300	294	289	44	229	16	0.850	0.023	0.567	0.259	20.41	6.14	0.379	0.280	0.341

Note: The values of  $V_{nano}$  and  $S_{nano}$ ,  $V_{meso}$  and  $S_{meso}$ , and  $V_{macro}$  and  $S_{macro}$  were calculated by integration of the  $f_V(R)$  and  $f_S(R)$  functions at  $0.35 \text{ nm} < R < 1 \text{ nm}$ ,  $1 \text{ nm} < R < 25 \text{ nm}$ , and  $25 \text{ nm} < R < 100 \text{ nm}$ , respectively. The values of  $\langle R_V \rangle$  and  $\langle R_S \rangle$  as the average pore radii were calculated as a ratio of the first moment of  $f_V(R)$  or  $f_S(R)$  to the zero moment (integration over the 0.35 to 100 nm range)  $\langle R \rangle = \int f(R)RdR / \int f(R)dR$ .  $D_i$  is the fractal dimension (Frenkel–Hill–Halsey method);  $c_{slit}$ ,  $c_{cyl}$ , and  $c_{void}$  are the weight constants calculated using the SCV/SCR method.

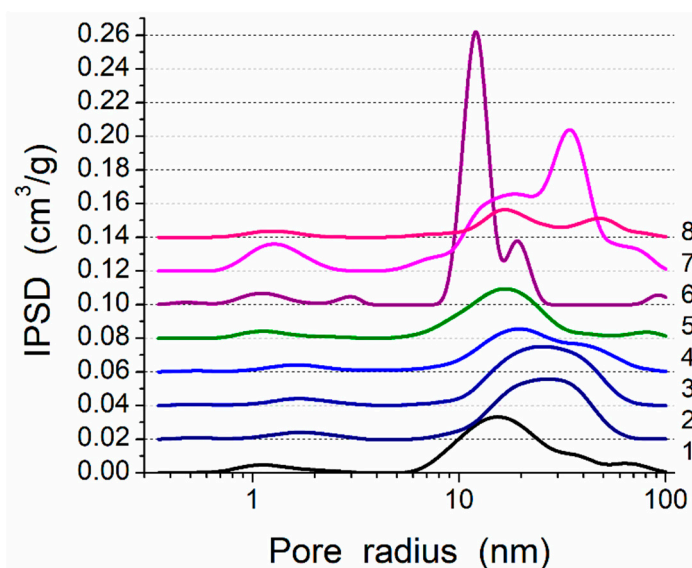


**Figure 3.** Incremental pore-size distributions (PSD) (SCV/SCR method) for PMS, A-300 and their blends (curve numbers correspond to sample numbers in Table 1).

Additionally, the nonlocal density functional theory (NLDFT, Quantachrome software (Quantachrome Instruments, Boynton Beach, FL, USA), with a model of cylindrical pores in silica [45]) method was used to calculate the differential PSD (Figure S6).

The main error in the evaluation of the textural characteristics such as the  $S_{BET}$  value based on the nitrogen adsorption isotherms is due to variation in the area ( $\sigma$ ) occupied by nitrogen molecules. It is assumed that  $\sigma = 0.162 \text{ nm}^2$ . This value is correct for graphite, but in the case of silica, it is smaller [46] due nonparallel location of  $N_2$  molecules with respect to the surface plane. Therefore, overestimation of the  $S_{BET}$  value could be 16% for silica. Despite this fact, in firm software  $\sigma = 0.162 \text{ nm}^2$ , and for simplicity, one can use this value because the effective  $\sigma$  value for various materials is different and unknown.

#### 2.4. $^1\text{H}$ MAS and $^{29}\text{Si}$ CP/MAS NMR Spectroscopy

Solid-state  $^1\text{H}$  MAS NMR spectra (Figure 4a) were recorded using an Agilent DD2 600 MHz NMR spectrometer (Agilent, Santa Clara, CA, USA, magnetic field strength 14.157 T). A powder sample was placed in a pencil-type zirconia rotor of 4.0 mm o.d. The spectra were recorded at a spinning speed of 8 kHz with a recycle delay of 5 s. The adamantane was used as the reference of the  $^1\text{H}$  chemical shift of proton resonance ( $\delta_{\text{H}}$ ).

Solid-state  $^{29}\text{Si}$  CP/MAS NMR spectra (Figure 4b) were recorded using the same NMR spectrometer at a resonance frequency of 199.13 MHz for  $^{29}\text{Si}$  using the cross-polarization (CP), magic-angle spinning (MAS), and high-power  $^1\text{H}$  decoupling. The spectra were recorded at a spinning speed of 8 kHz (4  $\mu\text{s}$   $90^\circ$  pulses), 2 ms CP pulse, and a recycle delay of 3 s. The Si signal of tetramethylsilane (TMS) at 0 ppm was used as the reference of the  $^{29}\text{Si}$  chemical shift ( $\delta(^{29}\text{Si})$ ) [2,47].

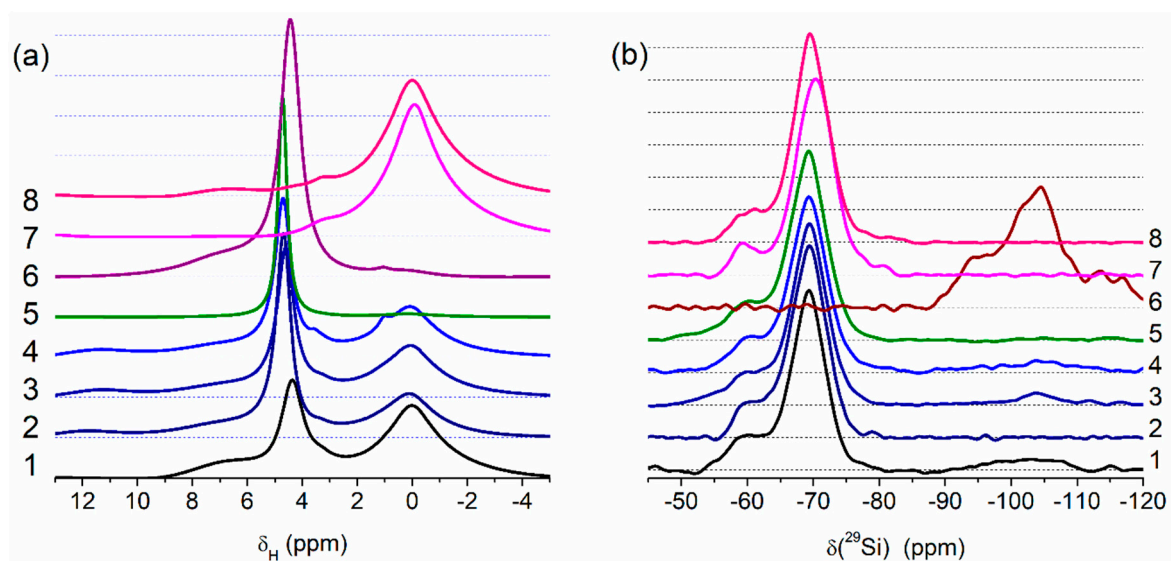


**Figure 4.** Solid state NMR spectra of (a)  $^1\text{H}$  (MAS) and (b)  $^{29}\text{Si}$  (CP/MAS) for PMS, A-300 and their blends (curve numbers correspond to sample numbers) ( $\text{Q}_n$  corresponds to  $\text{Si}(\text{OH})_{4-n}(\text{OSi}\equiv)_n$  at  $n = 2$  ( $-91\sim-93$  ppm), 3 ( $-99\sim-102$  ppm), and 4 ( $-109\sim-111$  ppm);  $\text{T}_3$  ( $-70$  ppm) corresponds to  $(\equiv\text{SiO})_3\text{SiCH}_3$  and  $\text{T}_2$  ( $-60$  ppm) corresponds to  $(\equiv\text{SiO})_2\text{Si}(\text{OH})\text{CH}_3$ , see Table S1).

### 2.5. Infrared Spectroscopy

The infrared (IR) spectra (Figure 5 and Figure S7) were recorded in the range of  $1800$  to  $300$   $\text{cm}^{-1}$  using a Specord M80 (Carl Zeiss AG, Oberkochen, Germany,  $4$   $\text{cm}^{-1}$  step, integration time of  $3$  s, the transmission spectra were converted into absorbance ones). Samples were carefully ground ( $5$  min) with KBr (Sigma-Aldrich, Saint Louis, MO, USA for spectroscopy) as 1:400 and pressed into thin pellets.

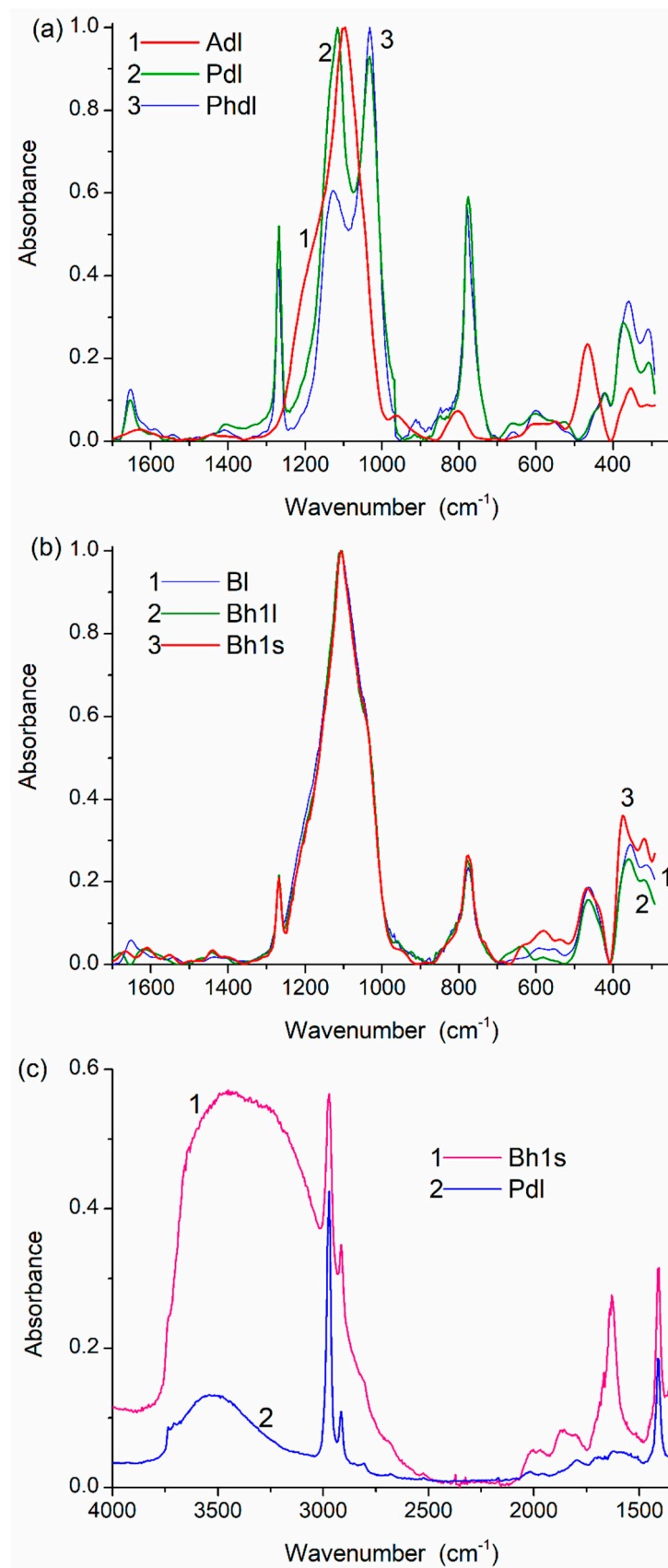


**Figure 5.** IR spectra of (a,c) PMS, A-300 and (b,c) their blends in the range of (a,b)  $1700\text{--}300\text{ cm}^{-1}$  and (c)  $4000\text{--}1300\text{ cm}^{-1}$ .



### 3. Results and Discussion

Simple stirring (without strong mechanical loading) of the dry PMS and dry cA-300 powders (Bl) results in good distribution of small nanosilica aggregates in the composite (Figure 1a, Figure 2a, Figures S1a, S3a and S4).

This composite is characterized by strong interactions between the PMS and silica nanoparticles because significant nonadditivity is observed for the textural characteristics of Bl in comparison to those of cA-300 (sample Adl) and dPMS (sample Pdl) (Table 1, Figure 3, Figures S5 and S6):  $S_{\text{BET}} = 186 \text{ m}^2/\text{g}$  instead of the expected  $(S_{\text{BET},\text{S6}} + S_{\text{BET},\text{S7}})/2 = 365 \text{ m}^2/\text{g}$  and  $V_{\text{p}} = 0.788 \text{ cm}^3/\text{g}$  instead of the expected  $1.556 \text{ cm}^3/\text{g}$ . This result could be explained by the embedding of small aggregates of silica nanoparticles into soft PMS (as light structures observed in larger PMS structures, Figure 1a and Figure S1a,b), and the grafting of PMS onto solid silica particles (similar to butter grafting onto macroporous bread resulting in a flat nonporous surface). If the silica aggregates could be remained at a surface of PMS particles that the strong decrease in the textural characteristics could be absent. The treatment changes the PSD in the total pore size range (Table 1,  $S_{\text{nano}}$ ,  $V_{\text{nano}}$ ,  $S_{\text{meso}}$ ,  $V_{\text{meso}}$ ,  $S_{\text{macro}}$ , and  $V_{\text{macro}}$ ); and the contributions of pores of different shapes change too (Table 1,  $c_{\text{slit}}$ ,  $c_{\text{cyl}}$ , and  $c_{\text{void}}$ ) in comparison to those of dry components (Adl and Pdl). A certain compaction of the blend is observed as a diminution of the  $\langle R_v \rangle$  value (Table 1).

The nitrogen adsorption isotherms (Figure S5) correspond to type II according to the IUPAC classification [48]. The desorption hysteresis shape provides clear evidence for formation of constricted, textural mesopores in sample 6 (various voids between particles). However, this is less visible for other samples having a simple shape of the hysteresis loops. The fact that the hysteresis loop for sample 7 (dPMS) does not close, probably indicates irreversible swelling of this material during nitrogen adsorption step, as well the presence of long pores with a narrow throat formed upon drying of the PMS hydrogel that results in additional cross-linking of the polymers due to condensation of residual silanols.

The addition of a small amount of water ( $h = 0.1 \text{ g/g}$ ) to the dry blend and stirring without strong mechanical loading results in slightly better homogenization (better embedding of A-300 aggregates into PMS and better PMS grafting onto silica) of the blend (Figures S1b and S3b), because water can play the role of a lubricant thus reducing the interactions of silica–silica and PMS–PMS. However, silica aggregates are visible in Bh1l as in Bl (Figure 1 and Figure S1).

There are certain changes in the textural characteristics of the Bh1l blend compared to Bl (Table 1, Figure 3, Figures S5 and S6), since both nanoporosity and mesoporosity decrease, but macroporosity increases due to reorganization of the secondary particles.

An increase in mechanical loading (Bh1s) leads to significant homogenization of the blend (Figure S1c), since silica aggregates (light structures) are not clearly visible as in Bl and Bh1l (Figure 1 and Figure S1a,b). This can be explained by decomposition of the aggregates upon stirring and stronger embedding of individual silica nanoparticles into the PMS matrix. There is a certain decrease in the nanoporosity (Table 1,  $S_{\text{nano}}$  and  $V_{\text{nano}}$ ) as well an increase in the macroporosity ( $S_{\text{macro}}$ ,  $V_{\text{macro}}$ , and  $\langle R_v \rangle$ ). The contributions of pores of different shapes slightly change (Table 1,  $c_{\text{slit}}$ ,  $c_{\text{cyl}}$ , and  $c_{\text{void}}$ ).

An increase in the amount of added water ( $h = 0.2 \text{ g/g}$ ) without strong mechanical loading (Bh2l) results in decreased porosity (water can fill the narrow pores and merge the particles together upon drying and degassing) (Table 1, Figure 3, Figures S5 and S6). However, the morphological changes are small (see Figures S1b,d, S2, S3b,d and S4) in comparison to Bh1l. Quantitative analysis of SEM images of samples Bl and Bh2s as representatives (Figure S4) shows that the mechanical treatment of a wetted blend results in decomposition of aggregates. This is appropriate for compaction of the blend observed in the textural characteristics (Table 1).

Enhanced mechanical loading (Bh2s) results in a strong diminution of the textural characteristics (Table 1), and the contributions of pores of different shapes change in comparison to Bh2l. Thus, upon stronger mechanical loading, the embedding-grafting effects increase in parallel to decomposition of silica aggregates, which are not visible similarly to Bh1s, but in contrast to Bl, Bh1l, and Bh2l.

Treatment of the hydrogel hPMS (drying, degassing) can give (Phdl) very strong compaction of the system (Table 1, Figures S5 and S6). However, this compaction occurs in domains (aggregates) because the relative contributions of the macropores ( $S_{\text{macro}}/S_{\text{BET}}$  and  $V_{\text{macro}}/V_{\text{p}}$ ) are maximal for Phdl (this process is similar to the strong drying of wet soil with the appearance of checks).

The results of the treatment processes appear in the solid-state NMR (Figure 4, Table S1) and IR (Figure 5) spectra. Treatment with the addition of water (resulting in better PMS grafting onto silica surface) reduces the intensity of the Q<sub>2</sub>–Q<sub>4</sub> lines, well observed for Adl (cA-300) (Table S1, Figure 4b).

The NMR spectra of water ( $\delta_{\text{H}} = 4\text{--}5$  ppm, Figure 4a) bound to PMS and the residual SiOH groups attached to =Si(CH<sub>3</sub>) (T<sub>2</sub> lines in Figure 4b) depend on the type of samples and their treatment conditions. The amounts of water bound to dry PMS (samples Pdl and Phdl, Figure 4a) are relatively small because the amounts of residual SiOH groups (Figure 4b, T<sub>2</sub> at  $-60$  ppm), which are the main adsorption sites for bound water, are relatively small (Table S1). The <sup>1</sup>H MAS NMR spectrum of cA-300 (Adl) demonstrates three lines at  $\delta_{\text{H}} \approx 7$  ppm (strongly disturbed silanols),  $\delta_{\text{H}} \approx 4\text{--}5$  ppm (water and disturbed silanols), and  $0\text{--}3$  ppm (free silanols). Interactions of PMS with a silica surface lead to diminution of relative content of strongly disturbed silanols (e.g., for Bh2s, only one signal is observed at  $4\text{--}5$  ppm). For sample Bh2s, the lines of the CH<sub>3</sub> groups (Figure 4a) and Q<sub>2</sub>–Q<sub>4</sub> (Figure 4b) lines are not observed.

The spectral changes and differences for the samples studied are observed in the IR spectra (Figure 5 and Figure S6). For example, samples of dry PMS (Pdl and Phdl) are characterized by practically identical bands of the symmetrical Si–O stretching vibrations at  $800\text{--}700$  cm<sup>-1</sup> (Figure 5a). However, the asymmetrical Si–O stretching vibrations are at  $1200\text{--}1000$  cm<sup>-1</sup> (especially at  $1130\text{--}1115$  cm<sup>-1</sup>) due to the difference in the cross-linking degree (compaction), the relative numbers of  $\equiv\text{SiO})_3\text{SiCH}_3$  (T<sub>3</sub>, Figure 4b, Table S1) and  $(\equiv\text{SiO})_2\text{Si(OH)CH}_3$  (T<sub>2</sub>), and the compaction type on drying (stronger check effects on drying of hPMS, Table 1). Water is stronger bound and in a larger amount in the blend than in dPMS alone (Figure 5c). The stirring effects more weakly appear in the IR spectra (Figure 5b) than in the textural characteristics or NMR spectra, because the IR spectra are transmission spectra of the total samples. The PMS-onto-silica grafting/embedding effect is therefore difficult to observe in the IR spectra.

Theoretical modeling (see Figures S8–S11 in ESM file) shows that PMS particles may be hydrated due to the presence of residual silanol groups appearing in the <sup>29</sup>Si CP/MAS NMR spectra (Figure 4b) as a line at  $-60$  ppm. This effect explains the good distribution of hydrated silica nanoparticles in the hydrated blends after significant mechanical loading (Figure 1 and Figures S2–S4). Note that the use of relatively small amounts of water ( $h = 0.1$  or  $0.2$  g/g) can prevent the formation of separate phases of PMS and A-300 upon mechanical treatment of the blends.

#### 4. Conclusions

The effects of adding amounts of water ( $0\text{--}0.5$  g of water per gram of dry solids) to the polymethylsiloxane/fumed silica blends (1:1 w/w) undergoing different mechanical treatment (stirring with weak ( $\sim 1\text{--}2$  kg/cm<sup>2</sup>) and strong ( $\sim 20$  kg/cm<sup>2</sup>) loading) were analyzed using TEM and SEM images, nitrogen adsorption–desorption isotherms (pore size distribution and other textural characteristics), solid-state NMR (<sup>1</sup>H MAS and <sup>29</sup>Si CP/MAS) spectra, and infrared spectra in the range of  $1700$  to  $300$  cm<sup>-1</sup> (related to the Si–O stretching vibrations). Both dry and wetted PMS (with 3D cross-linking in the particles containing residual SiOH and CH<sub>3</sub> group attached to each Si atoms) is a soft material, which can be grafted onto a silica surface, and silica aggregates can be embedded into the PMS matrix even upon weak mechanical loading. The main evidence of this effect is strongly nonadditive changes in the textural characteristics, which become two to three times smaller than additive those expected. All the PMS/nanosilica blends, demonstrating a good distribution of nanosilica nanoparticles and their small aggregates in the polymer matrix, are rather meso/microporous, with the main PSD peaks at  $R > 10$  nm and average  $\langle R_{\text{V}} \rangle$  values of  $18\text{--}25$  nm. Contributions of nanopores ( $R < 1$  nm), mesopores ( $1 \text{ nm} < R < 25$  nm), and macropores ( $25 \text{ nm} < R < 100$  nm) depend strongly on the type

of the materials (A-300, cA-300, dPMS, dried hPMS, and dPMS/cA-300 blends dried or wetted) and the type of treatment and amounts of added water. Thus, the developed technique allows one to significantly change the morphological and textural characteristics of fumed silica (hydrocompaction), PMS (drying–wetting–drying), and PMS/A-300 blends (wetting–drying under controlled mechanical loading), something that is of importance from a practical point of view.

**Supplementary Materials:** The following are available online at <http://www.mdpi.com/1996-1944/12/15/2409/s1>. Figure S1: TEM images of (a) Bl, (b) Bh1l, (c) Bh1s, (d) Bh2l, (e) Bh2s, (f) Adl, (g) Pdl, and (h) Phdl (scale bar 100 nm (a–d,h) and 200 nm (e,f)), Figure S2: TEM image of Bh2l, Figure S3: SEM images of Bl, (b) Bh1l, (c) Bh1s, (d) Bh2l, (e) Bh2s, (f) Adl, (g) Pdl, and (h) Phdl (scale bar 1  $\mu\text{m}$ ), Figure S4: Particle size distributions (PaSD) of samples 1 (Bl) and 5 (Bh2s) calculated using SEM images (Figure S3) and Fiji software with local thickness plugin (<https://imagej.net/Fiji>), Figure S5: Nitrogen adsorption-desorption isotherms (77.4 K) for PMS, cA-300, and their blends (curve numbers correspond to sample numbers of in Table S1), Figure S6: NLDFT PSD (equilibrium model with cylindrical pores in silica) for PMS, cA-300, and their blends (curve numbers correspond to sample numbers of Table S1), Table S1: Contributions of various structures in PMS, cA-300, and their blends, Figure S7: IR spectra (in the range of 1700–300  $\text{cm}^{-1}$ ) of dPMS/cA-300 blends differently hydrated before strong mechanical treatment (thin pallets were pressed using samples stirred with KBr as 1:400), Figure S8: Model of hydrated PMS nanoparticle (PM7 method), Figure S9: Model of hydrated silica nanoparticle (PM7 method), Figure S10: Model of two hydrated silica nanoparticles as a simple aggregate (PM7 method), Figure S11: Model  $^1\text{H}$  NMR spectra (PM7 + correlation function) of hydrated PMS (curve 1) and two nanosilica particles (curve 2); and experimental  $^1\text{H}$  NMR spectra of static PMS sample (curve 3) and nanosilica (curve 4,  $^1\text{H}$  MAS NMR).

**Author Contributions:** T.V.K., I.P., E.M.P., V.M.G., and V.V.T. conceived and designed the experiments; T.V.K., I.P., and D.Z. performed all the experiments; I.P., V.M.G., and V.V.T. analyzed and interpreted the data; I.P., V.G., and V.V.T. wrote the manuscript; Z.L. and W.D. contributed reagents/materials/analysis tools; all the authors revised and approved the final version of the manuscript.

**Funding:** I.P. is grateful to China Postdoctoral Science Foundation (grant No Z741020001), and Z.L. is grateful to Special Funding of the ‘Belt and Road’ International Cooperation of Zhejiang Province (grant No 2015C04005) for financial support.

**Availability of Data and Materials:** The datasets supporting the conclusions of this work are included within the article. Any raw data generated and/or analyzed in the present study are available from corresponding author on request.

**Conflicts of Interest:** The authors declare that they have no competing interests.

## Notations

Abbreviation	Full Name
$\text{SiO}_2$	Silica
PDMS	Poly(dimethylsiloxane)
PMS	Polymethylsiloxane
$S_{\text{BET}}$	Surface area
$\delta$	Chemical shift
CP/MAS NMR	Cross Polarization Magic-Angle Spinning Nuclear Magnetic Resonance
hPMS	hydrated polymethylsiloxane
dPMS	dehydrated polymethylsiloxane
$\rho_b$	bulk density
Bl	dPMS and dry cA-300 (1:1 w/w) mixed without strong mechanical loading
Bh1l	dPMS and dry cA-300 (1:1 w/w) mixed with an addition of distilled water without strong mechanical loading
Bh1s	dPMS and dry cA-300 (1:1 w/w) mixed with an addition of distilled water with strong mechanical loading
Bh2l	Water ( $h = 0.2$ g/g) was added to S1 sample; and the sample was stirred without strong mechanical loading

Bh2s	Bh2l was additionally stirred with strong mechanical loading for 10 min; Adl, dried and stirred cA-300
Pdl	Stirred dehydrated PMS
R	Pore radius
$\langle R_V \rangle$ and $\langle R_S \rangle$	The average pore radii with respect to the pore volume and specific surface area, respectively
PSD	Pore size distributions
$V_p$	Pore volume
$V_{\text{nano}}$	Volume of nanopores ( $R < 1$ nm)
$V_{\text{meso}}$	Volume of mesopores ( $1 \text{ nm} < R < 25$ nm)
$V_{\text{macro}}$	volume of macropores ( $25 \text{ nm} < R < 100$ nm)
$S_{\text{nano}}$	Specific surface area of nanopores ( $R < 1$ nm)
$S_{\text{meso}}$	Specific surface area of mesopores ( $1 \text{ nm} < R < 25$ nm)
$S_{\text{macro}}$	Specific surface area of macropores ( $25 \text{ nm} < R < 100$ nm)
$S_{\text{DFT/cyl}}$	NLDFT specific surface area with a model of cylindrical pores in silica
$c_{\text{slit}}$ , $c_{\text{cyl}}$ , and $c_{\text{void}}$	contributions of slit-shaped, cylindrical pores and voids between nonporous nanoparticles, the weight constants calculated using the SCV/SCR method
NLDFT	nonlocal density functional theory
TEM and SEM	Transmission and scanning electron microscopy; IR, infrared spectroscopy.

## References

- Iler, R.K. *The Chemistry of Silica: Solubility, Polymerization, Colloid and Surface Properties and Biochemistry of Silica*; Wiley: Chichester, UK, 1979; ISBN 978-0-471-02404-0.
- Legrand, A.P. *The Surface Properties of Silicas*, 1st ed.; Wiley: New York, NY, USA, 1998; ISBN 978-0471953326.
- Auner, N.; Weis, J. (Eds.) *Oganosilicon Chemistry VI: From Molecules to Materials*, 1st ed.; Wiley-VCH: Weinheim, Germany, 2005; ISBN 978-3527312146.
- Protsak, I.S.; Tertykh, V.A.; Pakhlov, E.M.; Derylo-Marczewska, A. Modification of fumed silica surface with mixtures of polyorganosiloxanes and dialkyl carbonates. *Prog. Org. Coat.* **2017**, *106*, 163–169. [[CrossRef](#)]
- Rao, A.V.; Kulkarni, M.; Amalnerkar, D.P.; Seth, T. Surface chemical modification of silica aerogels using various alkyl-alkoxy/chloro silanes. *Appl. Surf. Sci.* **2003**, *206*, 262–270. [[CrossRef](#)]
- Park, S.E.; Prasetyanto, E.A. Morphosynthesis and Catalysis by Organofunctionalized Mesoporous Materials. In *Organosilanes Properties Performance and Applications*; Wyman, E.B., Skief, M.C., Eds.; Nova Science Publishers: New York, NY, USA, 2010; pp. 101–131. ISBN 978-1-60876-452-5.
- Daoud, W.A.; Xin, J.H.; Xiaoming, T. Synthesis and characterization of hydrophobic silica nanocomposites. *Appl. Surf. Sci.* **2006**, *252*, 5368–5371. [[CrossRef](#)]
- Bernardoni, F.; Kouba, M.; Fadeev, A.Y. Effect of curvature on the packing and ordering of organosilane monolayers supported on solids. *Chem. Mater.* **2008**, *20*, 382–387. [[CrossRef](#)]
- Moitra, N.; Ichii, S.; Kamei, T.; Kanamori, K.; Zhu, Y.; Takeda, K.; Nakanishi, K.; Shimada, T. Surface Functionalization of Silica by Si–H Activation of Hydrosilanes. *J. Am. Chem. Soc.* **2014**, *136*, 11570–11573. [[CrossRef](#)] [[PubMed](#)]
- Li, Y.-F.; Xia, Y.-X.; Xu, D.-P.; Li, G.-L. Surface Reaction of Particulate Silica with Polydimethylsiloxanes. *J. Polym. Sci.* **1981**, *19*, 3069–3079. [[CrossRef](#)]
- Xiao, D.; Zhang, H.; Wirth, M. Chemical Modification of the Surface of Poly(dimethylsiloxane) by Atom-Transfer Radical Polymerization of Acrylamide. *Langmuir* **2002**, *18*, 9971–9976. [[CrossRef](#)]
- Protsak, I.S.; Kuzema, P.O.; Tertykh, V.A.; Bolbukh, Y.M.; Kozakevich, R.B. Thermogravimetric analysis of silicas chemically modified with products of deoligomerization of polydimethylsiloxane. *J. Therm. Anal. Calorim.* **2015**, *121*, 547–557. [[CrossRef](#)]
- Barandeh, F.; Nguyen, P.; Kumar, R.; Iacobucci, G.J.; Kuznicki, M.L.; Kosterman, A.; Bergey, E.J.; Prasad, P.N.; Gunawardena, S. Organically modified silica nanoparticles are biocompatible and can be targeted to neurons in vivo. *PLoS ONE* **2012**, *7*, e29424. [[CrossRef](#)]
- Dash, S.; Mishra, S.; Patel, S.; Mishra, B.K. Organically modified silica: Synthesis and applications due to its surface interaction with organic molecules. *Adv. Colloid Interface Sci.* **2008**, *140*, 77–94. [[CrossRef](#)]

15. Peng, P.; Lan, Y.; Luo, J. Modified silica incorporating into PDMS polymeric membranes for bioethanol selection. *Adv. Polym. Technol.* **2019**, *2019*, 5610282. [CrossRef]
16. Jung, H.S.; Moon, D.S.; Lee, J.K. Quantitative analysis and efficient surface modification of silica nanoparticles. *J. Nanomater.* **2012**, *2012*, 593471. [CrossRef]
17. Blitz, J.P.; Gun'ko, V.M. (Eds.) *Surface Chemistry in Biomedical and Environmental Science*; NATO Science Series II: Mathematics, Physics and Chemistry; Springer: Dordrecht, The Netherlands, 2006.
18. Finiels, B.; Alonso, M.; Bousmina, D.; Brunel, A.; Kadib, E. Periodic mesoporous organosilicas derived from amphiphilic bulky polymethylsiloxane. *New J. Chem.* **2016**, *40*, 4132–4135. [CrossRef]
19. Sharaf, M.A.; Mark, J.E. Modulus of randomly crosslinked polymethylsiloxane networks. *PMSE* **1993**, *68*, 180–181. [CrossRef]
20. Zhang, H.; Fidelis, L.C.; Serva, A.L.T.; Michaela, M.; Rezwani, K. Water-based freeze casting: Adjusting hydrophobic polymethylsiloxane for obtaining hierarchically ordered porous SiOC. *J. Am. Ceram. Soc.* **2017**, *100*, 1907–1918. [CrossRef]
21. Clarson, S.J.; Semlyen, J.A. Studies of Cyclic and Linear Poly(dimethylsiloxanes): 21. High Temperature Thermal Behavior. *Polymer* **1986**, *27*, 91–95. [CrossRef]
22. Krumpfer, J.W.; McCarthy, T.J. Rediscovering Silicones: “Unreactive” Silicones React with Inorganic Surfaces. *Langmuir* **2011**, *27*, 11514–11519. [CrossRef]
23. Barthel, H.; Nikitina, E. INS and IR study of Intermolecular Interactions at the Fumed Silica-Polydimethylsiloxane Interphase, Part 3. Silica-Siloxane Adsorption Complexes. *Silicon Chem.* **2004**, *1*, 261–279. [CrossRef]
24. Gun'ko, V.M.; Turov, V.V.; Zarko, V.I.; Goncharuk, E.V.; Gerashchenko, I.I.; Turova, A.A.; Mironyuk, I.F.; Leboda, R.; Skubiszewska-Zięba, J.; Janusz, W. Comparative characterization of polymethylsiloxane hydrogel and silylated fumed silica and silica gel. *J. Colloid Interface Sci.* **2007**, *308*, 142–156. [CrossRef]
25. Gun'ko, V.M.; Turov, V.V.; Krupska, T.V.; Protsak, I.S.; Borysenko, M.V.; Pakhlov, E.M. Polymethylsiloxane alone and in composition with nanosilica under various conditions. *J. Colloid Interface Sci.* **2019**, *541*, 213–225. [CrossRef]
26. Gun'ko, V.M.; Pakhlov, E.M.; Goncharuk, O.V.; Andriyko, L.S.; Marynin, A.I.; Ukrainets, A.I.; Charmas, B.; Skubiszewska-Zięba, J.; Blitz, J.P. Influence of hydrophobization of fumed oxides on interactions with polar and nonpolar adsorbates. *Appl. Surf. Sci.* **2017**, *423*, 855–868. [CrossRef]
27. Protsak, I.S.; Henderson, I.M.; Tertykh, V.A.; Dong, W.; Le, Z. Cleavage of organosiloxanes with dimethyl carbonate: A mild approach to graft-to-surface modification. *Langmuir* **2018**, *34*, 9719–9730. [CrossRef] [PubMed]
28. Protsak, I.S.; Morozov, Y.M.; Dong, W.; Le, Z.; Zhang, D.; Henderson, I.M. A <sup>29</sup>Si, <sup>1</sup>H, and <sup>13</sup>C Solid-State NMR Study on the Surface Species of Various Depolymerized Organosiloxanes at Silica Surface. *Nanoscale Res. Lett.* **2019**, *14*, 160. [CrossRef] [PubMed]
29. Nikolaev, V.G. *Enterogel: A Novel Organosilicon Enterosorbent with a Wide Range of Medical Applications*; Mikhailovsky, S., Khajibaev, A., Eds.; Springer: Berlin, Germany, 2011; pp. 199–221.
30. Shevchenko, Y.N.; Dushanin, B.M.; Yashinina, N.I. New Silicon Compounds Porous Organosilicon Matrices for Technology and Medicine. In *Silicon for the Chemistry Industry III*; The Norwegian University of Science and Technology: Sandefjord, Norway, 1996; ISBN 9788290265194.
31. Chaplin, M. Water Structure and Science. Available online: <http://www1.lsbu.ac.uk/water/> (accessed on 26 May 2019).
32. Mikheev, Y.A.; Guseva, L.N.; Davydov, E.Y.; Ershov, Y.A. The hydration of hydrophobic substances. *Russ. J. Phys. Chem. A* **2007**, *81*, 1897–1913. [CrossRef]
33. Yaminsky, V.V.; Vogler, E.A. Hydrophobic hydration. *Curr. Opin. Colloid Interface Sci.* **2001**, *6*, 342–349. [CrossRef]
34. Widom, B.; Bhimalapuram, P.; Koga, K. The hydrophobic effect. *PCCP* **2003**, *5*, 3085–3093. [CrossRef]
35. Chandler, D. Interfaces and the driving force of hydrophobic assembly. *Nature* **2005**, *437*, 640–647. [CrossRef]
36. Gun'ko, V.M.; Turov, V.V. *Nuclear Magnetic Resonance Studies of Interfacial Phenomena*; CRC Press: Boca Raton, FL, USA, 2013; ISBN 9781466551688.
37. Gun'ko, V.M.; Zarko, V.I.; Turov, V.V.; Leboda, R.; Chibowski, E. Distribution effect of the second phase in disperse silica/X oxides (X=Al<sub>2</sub>O<sub>3</sub>, TiO<sub>2</sub>, GeO<sub>2</sub>) on their surface properties. *Langmuir* **1999**, *15*, 5694–5702. [CrossRef]

38. Gun'ko, V.M.; Turov, V.V.; Pakhlov, E.M.; Krupska, T.V.; Borysenko, M.V.; Kartel, M.T.; Charmas, B. Water interactions with hydrophobic versus hydrophilic nanosilica. *Langmuir* **2018**, *34*, 12145–12153. [[CrossRef](#)]
39. Gun'ko, V.M.; Turov, V.V.; Protsak, I.S.; Krupska, T.V.; Pakhlov, E.M.; Tsapko, M.D. Effects of pre-adsorbed water on methane adsorption onto blends with hydrophobic and hydrophilic nanosilicas. *Colloids Surf. A Physicochem. Eng. Asp.* **2019**, *570*, 471–480. [[CrossRef](#)]
40. Chuiko, A.A. (Ed.) *Medical Chemistry and Clinical Application of Silicon Dioxide*; Naukova Dumka: Kiev, Ukraine, 2003; ISBN 966-00-0185-1. (In Russian)
41. Gun'ko, V.M.; Turov, V.V.; Pakhlov, E.M.; Krupska, T.V.; Charmas, B. Effect of water content on the characteristics of hydro-compacted nanosilica. *Appl. Surf. Sci.* **2018**, *459*, 171–178. [[CrossRef](#)]
42. Gregg, S.; Sing, K.S.W. *Adsorption, Surface Area and Porosity*; Academic Press: London, UK, 1982; ISBN 9780123009562.
43. Adamson, A.W.; Gast, A.P. *Physical Chemistry of Surface*; Wiley: New York, NY, USA, 1997; ISBN 978-0-471-14873-9.
44. Gun'ko, V.M. Composite materials: Textural characteristics. *Appl. Surf. Sci.* **2014**, *307*, 444–454. [[CrossRef](#)]
45. Neimark, A.V.; Ravikovitch, P.I. Capillary condensation in MMS and pore structure characterization. *Microporous Mesoporous Mater.* **2001**, *44*, 697–707. [[CrossRef](#)]
46. Thommes, M.; Köhn, R.; Fröba, M. Sorption and pore condensation behavior of pure fluids in mesoporous MCM-48 silica, MCM-41 silica, SBA-15 silica and controlled-pore glass at temperatures above and below the bulk triple point. *Appl. Surf. Sci.* **2002**, *196*, 239–249. [[CrossRef](#)]
47. Corminbœuf, C.; Heine, T.; Weber, J. <sup>29</sup>Si NMR chemical shifts of silane derivatives. *Chem. Phys. Lett.* **2002**, *357*, 1–7. [[CrossRef](#)]
48. Kruk, M.; Jaroniec, M. Gas adsorption characterization of ordered organic-inorganic nanocomposite materials. *Chem. Mater.* **2001**, *13*, 3169–3183. [[CrossRef](#)]



© 2019 by the authors. Licensee MDPI, Basel, Switzerland. This article is an open access article distributed under the terms and conditions of the Creative Commons Attribution (CC BY) license (<http://creativecommons.org/licenses/by/4.0/>).